Two-dimensional chemisorbed phases

L. D. Roelofs,[a] A. R. Kortan,[b] T. L. Einstein, and Robert L. Park

Department of Physics and Astronomy, University of Maryland, College Park, Maryland 20742

(Received 14 October 1980; accepted 2 January 1981)

Chemisorbed atoms on single-crystal metal surfaces frequently form commensurate diperiodic structures because of the strong, site-specific binding. Since the adatoms are well described by the lattice gas model, these systems are valuable testing grounds for recent theories of two-dimensional critical phenomena. We review briefly the developments in this field, emphasizing our results for the system O/Ni(111). This study includes an analysis of the multicritical low-coverage phase diagram, Monte Carlo simulations of the overlayer, and the first measurement of critical exponents for a phase transition in a chemisorbed overlayer probed via low energy electron diffraction. We compare our results with predictions of various two-dimensional models.

PACS numbers: 64.60.Fr, 68.20. + t, 75.40.Dy, 64.60.Cn

I. INTRODUCTION

There has been considerable theoretical interest and progress in the understanding of two-dimensional critical phenomena. It is now realized that 2-d critical transitions can be sorted by the symmetry of the ordered state into a small number of "universality classes." Within each class, members are expected to exhibit identical critical exponents, which have been theoretically determined approximately and in some cases exactly.[1] These developments have stimulated the search for physical systems to which the theories apply and the refinement of experimental methods for their study. The universality classes are typically labeled by the idealized magnetic model in the class,[2] because these models are more amenable to theoretical treatment than other members of the universality class. Since real 2-d magnets are rare, experimental efforts have concentrated on 2-d lattice gases, especially the adsorption of one atomic or molecular species onto a crystalline surface of another material.

Physisorption, discussed in the previous paper,[3] has quite different characteristic energies from chemisorption, leading to qualitative differences in the adatom phase transitions. In chemisorption, the lateral interactions between adatoms are smaller, often much smaller, than the "corrugations" on the surface, i.e., the energy difference between bonding in the most attractive sites and somewhere along the pathway between such sites. Hence, chemisorbed atoms are confined to a 2-d lattice of sites, making the lattice gas model[4] a very appropriate description. In physisorption, these two characteristic energies are comparable or reversed in order, allowing incommensurate structures, with adatoms in energetically unfavorable sites within the domain wall.[5] (When the corrugation is a small or negligible perturbation, still another qualitative regime occurs.[6])

The differing adsorption mechanisms in the two limits, related to the degree of electronic coupling to the substrate, causes a drastic difference in the adatom–adatom interactions. In physisorption the binding to the surface is a small perturbation on the free atom interactions; hence, a Lennard–Jones form can be used.[7] By contrast the interactions in the chemisorption case proceed via the substrate electronic states[8] and hence are much more difficult to characterize or calculate. Although model calculations[8,9] correctly predict the order of magnitude and relative strengths of such interactions, no quantitative methods are yet available for real systems. In this case the phase diagram of the overlayer can be used to determine adatom–adatom interactions through Monte Carlo simulation.[10–13]

Since the binding energy in chemisorption is much larger than the lateral interactions responsible for critical phenomena, negligible desorption occurs near the phase transition. The adatom number (i.e. fractional coverage) is constant, realizing the canonical ensemble viewpoint. In physisorption, both these characteristic energies are due to van der Waals forces. One must consider the bound adatoms in equilibrium with a surrounding vapor; the chemical potential is fixed, making a grand canonical ensemble appropriate.

One final difference of experimental significance is that because of the greater strength of the interactions in a chemisorption system, the phase transition temperatures tend to be higher and thus more accessible. Also critical regions, which scale with transition temperatures, are proportionally larger, easing the temperature control requirements.

For the lattice gas model to accurately describe chemisorbed atoms, the substrate must stay completely rigid and impenetrable, providing a 2-d net of sites. Reconstruction, whether spontaneous or adsorption-induced, removes the transitions from the 2-d universality classes. Such behavior, which for our purposes is highly undesirable, has stirred much recent interest for several (100) bcc metals.[14–17] A less dramatic complication is bulk dissolution. As with desorption, this new degree of freedom can be included implicitly in a lattice gas Hamiltonian via the chemical potential, but only if the surface is in equilibrium with the dissolved material, an extremely unlikely situation. Finally, the lattice gas picture can be destroyed by a reaction between adatoms and surface atoms which wrenches the latter from their original positions. In the case of oxygen chemisorbed on Ni(111), which will be considered in detail in this paper, such oxidation of the surface begins at coverages of about 0.4.[18,19]

Since there is an excellent review of the many studies of cooperative phenomena within chemisorbed overlayers,[20] we will focus on this particular system, O/Ni(111), which we have studied from an exceptionally large number of viewpoints.

 0022-5355/81/020492-08$01.00

We describe our experimental methods and results in Sec. II, our Monte Carlo simulations and results in Sec. III, and the measurement and analysis of the critical exponents of one order–disorder transition occurring in this system in Sec. IV. We conclude with a brief discussion of our results and future directions.

II. EXPERIMENT

A. Method

The experiments[19,21] were carried out in a UHV stainless steel bell jar system with total base pressure less than 10^{-10} Torr (10^{-8} Pa). A quadrupole mass analyzer was used to monitor the composition of gases in the system. A standard four-grid LEED optics system was used for all measurements. It was operated in the retarding mode to obtain the Auger electron spectrum which provided a relative oxygen coverage measurement. The coverage measurements were calibrated by assuming the maximum intensity of the $p(2 \times 2)$ beams occurs at $\theta = 0.25$. Work function changes were determined from the low-energy cutoff of the secondary electron spectrum.

Experiments were performed using five different samples, all of which were nominally 99.995% pure. Initially the samples exhibited mosaic spreads of 30 to 60 min. Two of the samples, however, were zone-refined to eliminate the mosaic spread and oriented to the (111) direction to better than 20 min. The results presented here, except for the critical exponent measurements, were found not to depend on the mosaic spread.

Prior to any measurements the samples were cleaned by argon-ion sputtering and annealed at 1000 K. Oxygen exposures of the clean sample were conducted at pressures in the range [10^{-9}–10^{-10} Torr] and at temperature 274 K. The temperature was measured by a calibrated chromel–alumel thermocouple. The output of the thermocouple provided feedback for the circuit which controlled the current to the sample heater. Liquid N_2 cooling allowed measurements to be made down to a temperature of 100 K. The stability of the temperature control system was ±0.01 K at 400 K.

Experimental feasibility requires different probes for chemisorption and physisorption studies. Most phase-transition experiments on physisorption systems have been carried out using calorimetric and vapor pressure measurements,[22] or neutron[23] or x-ray[24] diffraction. These methods are usually applied to high surface area materials, principally exfoliated graphite. By contrast, most chemisorption studies have used single crystals as substrates and a strongly interacting probe, usually low energy electron diffraction (LEED), to obtain surface sensitivity. LEED has also been applied successfully to some physisorption systems.[5,25] The advantages of this approach are the convenience of electron diffraction studies using modern LEED apparatus and the large defect-free regions that can be obtained on the surface of a single crystal. This reduces the importance of finite-size effects.[26] The disadvantage of electron scattering is the presence of multiple scattering effects, which complicate the extraction of the thermodynamically interesting pair correlation function. However, the relatively small probability for right-angle scattering[27] reduces the importance of higher-order scatterings *within* the overlayer. As a result the diffraction beam profiles are the Fourier-transformed pair correlation function modulated by a slowly varying envelope arising from interplanar multiple scattering.[28] Therefore, careful measurement of LEED profiles allows the extraction of critical exponents.

We used an optical system mounted external to the vacuum system to project a real image of a given diffraction beam onto the aperture of a photon counter. The angular profile of the beam was obtained by varying the incident beam energy to move the beam across the aperture. The equivalent angle of acceptance of the aperture was 1°.

B. Results

At room temperatures and low coverages, oxygen adsorption results in no new diffraction features. As the coverage approaches $\frac{1}{4}$ (all coverages are given in monolayers), however, the oxygen orders into a $p(2 \times 2)$ phase. The linear increase of work function with coverage suggests that at all coverages the oxygen atoms occupy the same sites, a necessary property for ideal lattice gas description. As mentioned above, NiO begins to form at $\theta = 0.4$ and above $T = 500$ K oxygen diffuses into the Ni crystal. These properties defined the limits of our study of the 2-d cooperative effects within the overlayer.

To obtain the phase diagram, the surface was exposed at $T = 273$ K to reach a given relative coverage, as indicated by Auger electron spectroscopy. The temperature was then varied between the limits 100–500 K while the changes in the LEED pattern were monitored.

No changes were observed in the work function or Auger signal while varying the temperature. LEED, however, revealed many changes. An ordered $p(2 \times 2)$ structure could be obtained for coverages well below $\frac{1}{4}$ by lowering the temperature sufficiently. The integral order diffraction beams were unaffected by temperature changes, except for the Debye–Waller effect. In contrast, the half-order diffraction beams, arising from the double-spaced overlayer, broadened and disappeared above a transition temperature. This behavior is characteristic of island formation resulting from an attractive interaction, in this case the third-nearest neighbor interaction. Similar island formation and dissolution have been studied by Lagally and co-workers for O/W(110).[29] As the coverage approaches a quarter of a monolayer the transition temperature rises very abruptly. The transition becomes sharper and the beam broadening more abrupt in this region, indicating the transition is critical (second order). It was this transition which was studied in detail to determine associated exponents (see Sec. IV).

When the oxygen coverage is increased above about 0.27, some interesting changes take place in the LEED pattern. As depicted in Fig. 1, the half-order beams broaden, the (1/2,1) beams split into two components along the (0,1) directions while the (1/2,0) beams merely broaden. The four characteristic lengths describing splitting and broadening in the LEED pattern, denoted by lower case Greek letters in the figure, all increase continuously with coverage above $\theta = 0.27$. The severe broadening of diffraction beams indicates a loss of order on the scale of 100 Å. However, their persistence

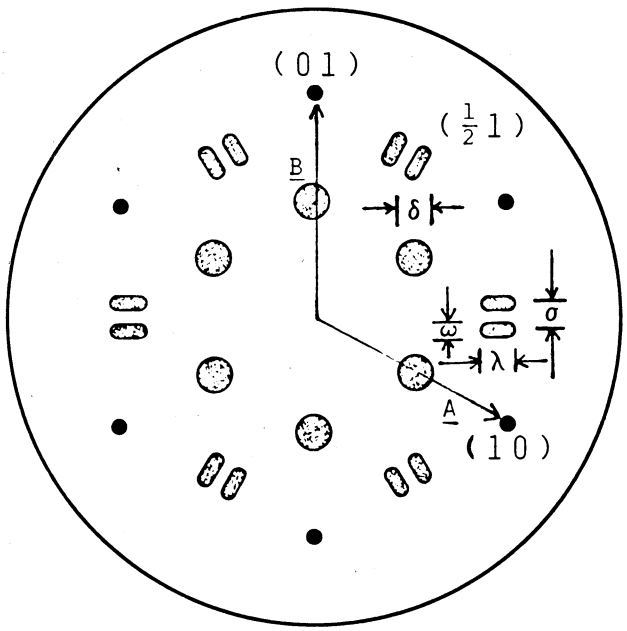

FIG. 1. Schematic LEED beam pattern for the intermediate structure found at coverages between 0.27 and 0.29. The (1/2,0) beams broaden circularly, while the (1/2,1) beams split and elongate. A and B are the reciprocal lattice vectors of the Ni surface. The (0,0) beam is obscured by the sample holder.

discloses some short-range order, which provides valuable information about local correlations.

Marcus *et al.*[31] concluded on the basis of dynamical LEED analysis of the $p(2 \times 2)$ phase that the oxygen atoms occupy threefold hollows on the Ni(111) surface (see Fig. 2). There are, however, two types of these sites: hcp sites directly above a second-layer Ni atom and fcc sites directly above a vacancy in the second layer. The LEED calculations were unable to distinguish between these two possibilities.

In fact to explain the partially ordered LEED pattern of Fig. 1 it is necessary to place adatoms in both such sites.[30] (Since the (1/2,0) and (1/2,1) beams, which differ by substrate reciprocal lattice vector **B**, are strikingly different, the pattern cannot be formed in either the fcc or hcp sites alone.) The structure has regions of $p(2 \times 2)$ in the fcc sites adjoining regions $p(2 \times 2)$ in the hcp sites. The antiphase boundaries separating these regions are approximately equally spaced to give the splitting of the (1/2,1) beam. The formation of these boundaries allows extra oxygen atoms to adsorb while still maintaining many of the favorable third-nearest-neighbor bonds. Since the domain boundaries tend to parallel one of the three principal directions on the surface, the observed pattern is the superposition of the three equivalent orientations of the structure.

At a coverage of about 0.29, a set of sharp $(\sqrt{3} \times \sqrt{3})R30°$ beams appear in coexistence with the structure of Fig. 1. When the antiphase domain boundaries are forced sufficiently close by the increasing coverage, the $(\sqrt{3} \times \sqrt{3})R30°$ structure apparently becomes more favorable and forms in large regions on the surface. As θ increases above 0.29, the intensity of the contribution like Fig. 1 diminishes.

The pure $(\sqrt{3} \times \sqrt{3})R30°$ disorders at about $T = 300$ K. This transition is first-order as indicated by the hysteresis and the absence of beam broadening near the transition point.

All this information is summarized in the phase diagram shown in Fig. 3. The sharp rise in the transition temperature near $\theta = 0.21$ strongly suggests the presence of a tricritical point.[31] The phase boundary separating the long-range ordered $p(2 \times 2)$ gas coexistence region is conjectured. Recent work by Cardy *et al.*[32] suggests that the coexistence region might approach the tricritical point with a cusp-like shape. The sample cooling arrangement restricted data acquisition to above 100 K, but the equilibration time of the overlayer becomes prohibitively long not far below this temperature anyway.

III. MONTE CARLO SIMULATION

A. Method

The results of the LEED study described in the previous section imply that the lattice of sites occupied by oxygen atoms has hexagonal symmetry. We developed a Monte Carlo simulation program to reproduce the experimental phase diagram. This program, which is the first to treat this symmetry, is written partly in machine language to achieve the economy necessary for generating full phase diagrams and is described in detail elsewhere.[30] In this procedure, a predetermined number of lateral interactions between adatoms are the input parameters; they are adjusted to optimize reproduction of the actual phase diagram. Leaving out significant interactions causes misleading results in the simulation, in which large

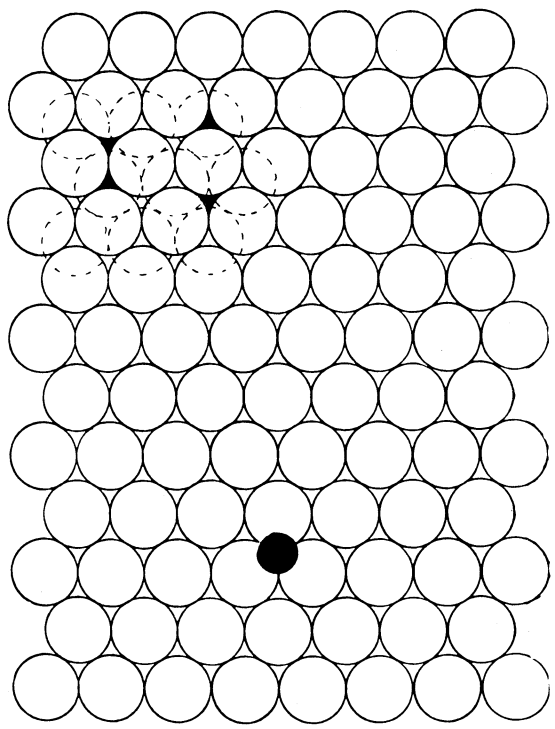

FIG. 2. Oxygen binding sites on the nickel surface. Ni atoms are open circles. The solid circle represents an oxygen atom adsorbed into a threefold site on the surface. In the lower right a few second layer nickel atoms are shown (dashed circles) to show the difference between fcc sites (upward pointing 'triangles') and hcp sites (downward pointing 'triangles'). Two of each are darkened.

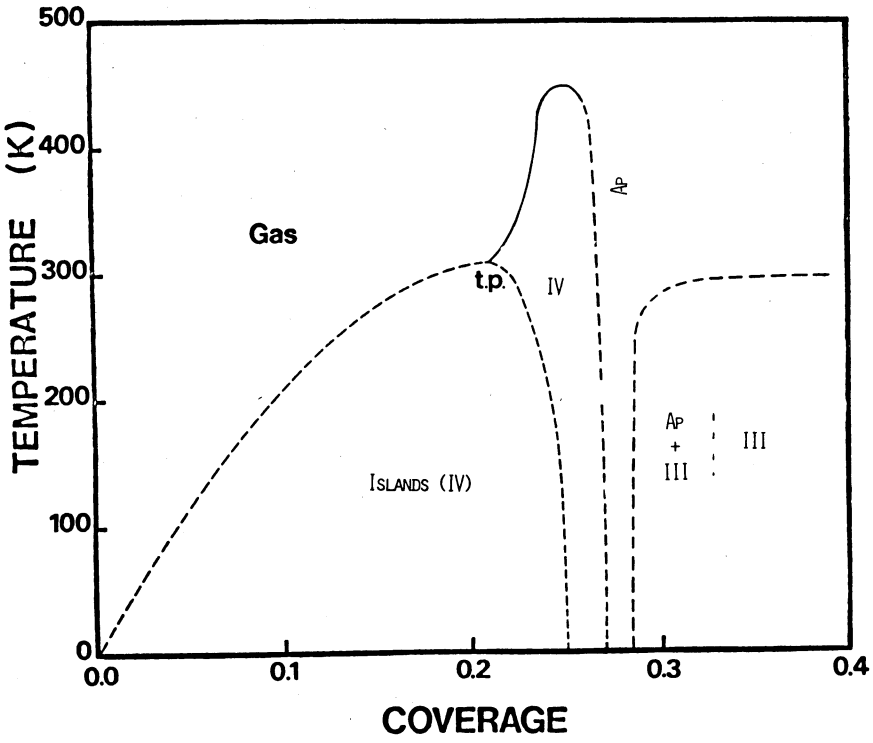

FIG. 3. Phase diagram for oxygen adsorbed on Ni(111). The solid line denotes a continuous phase transition, while the dashed lines indicate first-order transitions. The ordered phases are labeled according to the following convention. The inverse saturation density of the ordered phase is given as a Roman numeral. Thus IV denotes $p(2 \times 2)$ ($\theta_{sat} = 0.25$) and III denotes $(\sqrt{3} \times \sqrt{3})R30°$ ($\theta_{sat} = 0.333$). Ap denotes the antiphase domain phase described in Sec. II. Islands (III) is a coexistence of the Gas and (IV) regions and (Ap + III) is a coexistence of the antiphase domain and $(\sqrt{3} \times \sqrt{3})R30°$ structures.

fractions of the deduced values come from neglected interactions times some mean correlation function. Generally the longest distance interaction which must be included is that of the shortest pair of occupied sites in the lowest density ordered phase, since that energy usually characterizes the stability of that phase. Thus, in our case, the presence of the $p(2 \times 2)$ phase requires the inclusion of the third-neighbor interaction E_3 (see Fig. 4). Since low coverage islands form, E_3 is negative (attractive). Shorter-range interactions are generally greater in magnitude and influence the nature of disordering. In this case there is also a binding energy difference E_0 between fcc and hcp sites. Since the existence of the antiphase domain phase implies that E_0 is small compared to the shorter-range pair interactions, we assume that the pairwise interactions of given separation are the same regardless of binding site. In all, then, besides E_0, six distinct lateral interactions were included, the largest number in any simulation to date. F_0 was taken to be $+\infty$ by prohibiting any pairs of that type in the simulation. The distance involved, 0.73 Å, is such that strong overlap repulsions would occur.

Although the goal of this work was to determine the adatom interactions for O/Ni(111), a more fundamental conclusion regarding the binding site assignments was obtained. It was found that the complete phase diagram of Fig. 3 cannot be reproduced under the assumption of any one set of interaction energies. The results, however, suggest that a change in allowed binding sites may occur above coverage 0.25. Interestingly, all pair interactions but E_3 proved to be repulsive, many weakly so; van der Waals interactions are strongly repulsive at the shortest spacings and elsewhere attractive.

B. Results

Five full low-coverage phase diagrams and several more partial ones were generated. Figure 5, which is the phase diagram based on the first trial for the interaction energies (see caption), is representative.[33] Comparison of Figs. 3 and 5 shows that simulation correctly reproduced all observed phases and placed them in approximately correct relative positions. (The overall temperature scale must be fixed from experiment and the same ratio applied to all the interaction energies.) Even the antiphase domain phase (Ap) is reproduced, although the simulated LEED pattern of this structure did not show complete splitting of the (1/2,1) beam but rather partial splitting. It was found, however, that complete splitting could be achieved by reducing the binding energy difference, E_0, from its already small value.

One important feature of the experimental phase diagram,

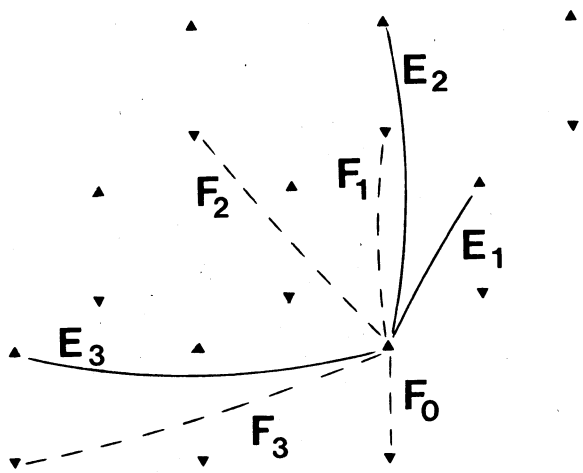

FIG. 4. Pairwise, hexagonal-lattice adatom interactions included in the simulation of O/Ni(111). Solid lines (and letter 'E') denote interactions between sites on the same sublattice and dashed lines (letter 'F') denote those between different type sites. Also included (but not shown) is a binding energy difference between fcc (triangles pointing upward) sites and hcp (triangles pointing downward). The effects of F_3 were not considered. (It was set to 0.)

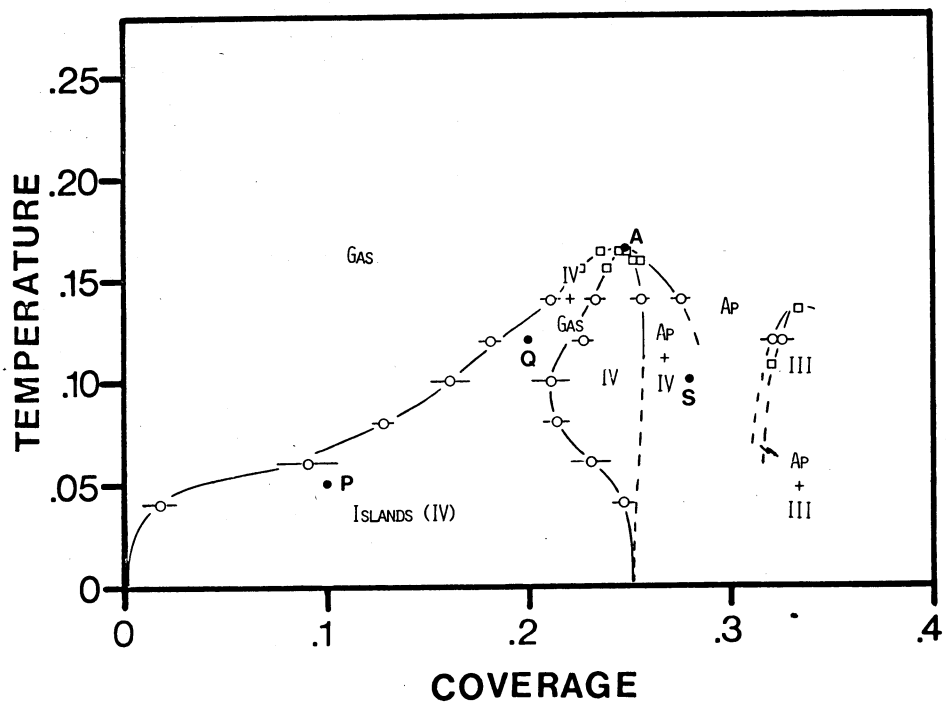

FIG. 5. Simulated hexagonal-lattice phase diagram for first assumed set of 'interactions': $F_0 = +\infty$, $E_1 = 1.0$, $F_1 = 0.667$, $E_2 = 0.05$, $F_2 = 0.167$, $E_3 = -0.06$, $E_0 = 0.05$. All transitions are first order.

however, could not be duplicated, namely the continuous second-order transitions from $p(2 \times 2)$ to gas near coverage 0.25. The first-order nature of this transition in Fig. 5 is indicated by the coexistence region which extends all the way to the maximum in the phase boundary. We were unable to force this transition to become second-order without increasing E_0 to a value comparable to E_1! Variations in the other interaction energies did not modify this result.[30]

C. Discussion

The crux of the difficulty in the simulations is establishing the value of E_0, which must be small for the formation of the antiphase domain phase and large to allow the $p(2 \times 2)$-gas transition to be second-order. A possible explanation is that for coverages below and equal to 0.25 only one of the two types of binding sites is allowed. The lattice in that case is triangular and our simulations of that symmetry have shown that the transitions from $p(2 \times 2)$-gas are second order,[30] and that for $\theta < 0.25$ the phase diagram can be accurately reproduced. We speculate then that it is not until $\theta = 0.27$ that both types of sites are occupied. This would require some transformation involving the Ni substrate, perhaps a reconstruction. The new set of conditions, by allowing occupation of both types of sites, would allow the formation of the antiphase domain structure. Such a transformation might also affect the other interaction energies significantly; however, to form the antiphase domain structure, E_3 should still be attractive. No further variations are necessary to explain the $(\sqrt{3} \times \sqrt{3})R30°$ phase, whose transitions are first order in both the simulation and the experiment. An experimental check of these speculations, for example, by more precise work function measurements as a function of *coverage*, is still necessary, since the possibility of substrate changes was not anticipated when the experiments were performed. We did not observe any changes at the 5% level in the integral beam I–V profiles.

Our findings vis-à-vis the order of transitions in the triangular and hexagonal systems are consistent with the predictions of Domany and Schick[34] based on Landau–Ginzburg–Wilson Hamiltonian classification schemes. It may then be that the lattice gas approximation with a single set of interactions is not tenable throughout the full low coverage (0–0.4 monolayers) regime for this system. In this case the system may be adequately described within a lattice gas framework within more restricted regimes, i.e., one set of parameters for $\theta < 0.27$ and another for $\theta > 0.27$. In the next section we discuss our measurements of critical exponents for the $p(2 \times 2)$ gas order–disorder transition at $\theta = 0.25$.

IV. THE $p(2 \times 2)$ ORDER–DISORDER TRANSITION

A. Analysis of data

As pointed out in the second section, near $\theta = 0.25$, the $p(2 \times 2)$ structure disorders via a reversible second-order transition. According to Domany *et al.*,[34] if the symmetry of the lattice is triangular, this continuous transition should lie in the four-state Potts universality class, in which case the exponents are known. To test this prediction, diffraction beam profiles were measured at closely spaced temperature intervals through the transition region. The diffraction beam profiles consist of the sum of a δ-function contributed by the long-range order ($T < T_c$ only) and a nearly Lorentzian contribution resulting from the scattering from short-range order.[35] This sum is then broadened by convolution with an instrument response function.[12,36] The broadening effect of the LEED instrument limits the range on the surface over which the pair correlation function is probed. The instrument response function was taken to be the measured beam profile at very low temperatures. It was deconvoluted from each higher temperature profile by two different methods.[30] To reduce truncation effects each profile was analytically extended and

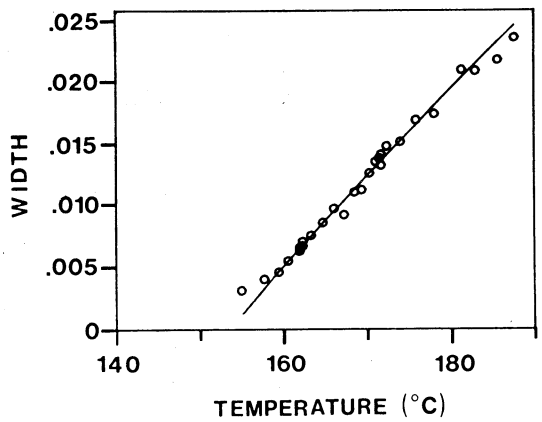

FIG. 6. Beam width (inverse correlation length) and power law fit (solid line) to the data to obtain the exponent ν.

a uniform background was subtracted. We also compensated for the Debye–Waller dependence of the intensity, which arises from disorder of the adatoms within their binding wells and is a non-lattice gas and noncooperative effect. In fact, of course, the extent of the long range order in the $p(2 \times 2)$ structure was limited by the degree of perfection of the substrate. Steps are thought to be the dominant limitation to the long-range order in our crystals.

As discussed in Sec. II.A, the use of LEED requires consideration of the effects of multiple scattering, but the only effect is a modulation of the beam intensity as a function of energy (or angle). This modulation is slowly varying on the scale of a typical beam width. We analyzed the data two ways. In one case we assumed no correction resulting from intensity–voltage (I–V) variation and in the other we used the I–V plot of the beam as an approximation to the modulating function.[37] Because of the relatively slow variation the results agreed well within the errors resulting from other effects.

To compare the observed order–disorder transition with the theoretical prediction we determined three critical exponents from the variation of the diffraction beam profiles near T_c. The exponent β, which describes the variation of the order parameter, was obtained from the amplitude of the long-range order component of the intensity. The exponent ν, which gives the behavior of the correlation length, was obtained from the width of the short-range order part of the intensity. (Hence there is rapid broadening of the beams above T_c.) The exponent γ, which describes the divergence of the intensity of critical (i.e., short-range) scattering (analogous to the susceptibility in a magnetic phase transition), was obtained from the amplitude of the short-range order part of the intensity.

The individual diffraction beam profiles were analyzed in two different ways. The first method consisted of Fourier space deconvolution of the 2-d profiles. The Bragg (long-range order) intensity was separated as the uniform background of the transformed deconvoluted profiles. In the second method, the sum of a δ function and a Lorentzian was convoluted with the measured instrument response function. The width and amplitude of the Lorentzian and the amplitude of the δ function were adjusted by nonlinear curve fitting techniques[38] to obtain the least squares fit to the measured profiles. For $T < T_c$, the two methods give good agreement for the Bragg intensity. For $T > T_c$, the second method is superior since truncation oscillations occur in the transforms. By assuming that the critical scattering contribution can be represented by a Lorentzian, the second method ignores line shape corrections described by the exponent η. We found, however, that our results were insensitive to the use of a function with $\eta \neq 0$. Table I gives our results for ν, γ, and β and displays relevant values from some model systems.[39]

Fitting to obtain the exponents is done by nonlinear curve-fitting techniques[38] using simple power law forms

$$Q = A|(T - T_c)/T_c|^{\lambda},$$

where A is the amplitude, λ is the critical exponent, T_c is the transition temperature, and Q is the quantity being fit. Note that there are three fitting parameters, A, λ, and T_c. A representative fit (exponent ν) is shown in Fig. 6. The data points (circles) representing the width of the critical part of the intensity were obtained using the second method of analysis. The points between temperatures 160° and 179°C were included in the fit. The fit gave $T_c = 153.7$°C. The fit for γ gave a consistent transition temperature $T_c = 153.9$°C. The fit for β was more sensitive to error since fewer data points were obtained for $T < T_c$ and since fits to small exponents seem to be more fragile. A fit in which T_c was allowed to vary gives $T_c = 156.4$ and $\beta = 0.16$. We feel, however, it is more accurate to fix T_c at the value determined from the ν and γ fits ($T_c = 154$°C) and in that case obtained the result $\beta = 0.14$. The rather large errors estimated for β take into account this sensitivity to T_c. The error bars quoted in Table I reflect the variations caused by changes in the fitting interval and statistical error estimated from the "goodness of fit."

B. Discussion

Table I indicates that the experimental results do not substantiate the assignment of this transition to the four-state Potts universality class.[40] Furthermore, the exponents also do not agree with four-state Potts exponents with Fisher renormalization (FR).[41] Since phase transitions in chemisorbed layers occur at fixed coverage (rather than fixed chemical potential, the field conjugate to the coverage), FR might in general be applicable. However, the region over which FR is applicable shrinks as one approaches the extremum ($dT_c/d\theta = 0$) in the phase boundary, since at an extremum the coverage does not vary with temperature (at fixed chemical potential). Our measurements were done as close to the extremum as possible since there the transition is most reproducible, the mobility is highest, and the critical region is largest. Thus FR does not apply in our case.

TABLE I. Exponent results, with model values for comparison.

Exponent	Magnetic measurable	Ising	4-state Potts	Potts F. R.[a]	O/Ni(111) $p(2 \times 2)$
α	Specific heat	0	$\frac{2}{3}$	2	N.M.[b]
β	Magnetization	$\frac{1}{8}$	$\frac{1}{12}$	$\frac{1}{4}$	0.14 ± 0.02
γ	Susceptibility	$\frac{7}{4}$	$\frac{7}{6}$	$\frac{7}{2}$	1.9 ± 0.2
ν	Correl. length	1	$\frac{2}{3}$	2	0.94 ± 0.1

[a] F.R.—Fisher renormalization
[b] N.M.—Not measured

Before considering the tantalizing agreement with Ising exponents, we mention two reasons why the experiment may not have obtained the correct exponents for the system. First it is not known how close to T_c one must be to see four-state Potts exponents. In our experiment the data range analyzed is 0.015–0.06 in terms of the reduced temperature $t \equiv |(T - T_c)/T_c|$. For an Ising transition, this range would give the exponents to within 5%[30]; for the Potts model, the corresponding percentage error is not known.

Another more intriguing possibility is the effect of logarithmic corrections[32,42] which occur because of an essential singularity as a function of q in the dilute q-state Potts models at $q = 4$.[43] Logarithmic corrections would also shift the effective values of the exponents. Since these corrections are not universal,[42] it is presently unclear whether they apply to the $p(2 \times 2)$ order–disorder transition. Further theoretical and experimental work is needed.

Returning at last to the agreement with the Ising exponents, we must again consider two scenarios. The first possibility is that the transition really does belong to the Ising universality class. The four-state Potts prediction physically arises from the four $p(2 \times 2)$ sublattices into which the triangular lattice may be divided.[40] The ordered state and any fluctuations out of it can occur in any of the four degenerate sublattices. If two of these sublattices were systematically rendered unfavorable, perhaps by steps[44] or other defects, Ising behavior might result. The second possibility is that in crossing over to four-state Potts exponents as $T \to T_c$, the exponents pass through Ising values. This possibility is being checked by Monte Carlo simulation.

V. CONCLUSION

We have seen that chemisorbed overlayers provide stimulating realizations of two-dimensional lattice gas models. They thus offer an area in which experimental, theoretical solid state and statistical mechanics expertise can all be fruitfully applied. The experimental obstacles are the current limitations on the coherence of the LEED apparatus and on sample perfection. Theoretical treatment is necessary to elucidate questions of sizes of critical regions, crossover behavior, applicability of logarithmic corrections, etc. To round out the understanding, it would be useful to determine the adatom interactions, binding sites and the likelihood of substrate involvement in phase transitions from first principles.

ACKNOWLEDGMENTS

We are grateful for very helpful discussions with Professors A. N. Berker, M. G. Lagally, J. Nicoll, and M. Schick, and Dr. J. S. Walker. One of us (LDR) wishes to acknowledge the support of the Brown University Materials Research Laboratory during the preparation of this manuscript. LDR at Maryland and TLE were supported by the Department of Energy under Grant DE AS05-79ER-10427. Computer time and facilities were provided by the University of Maryland Computer Science Center. ARK and RLP were supported by the National Science Foundation under Grant DMR 7900323.

[a]Present address: Physics Dept., Brown University, Providence, RI 02912.
[b]Present address: Physics Dept., MIT, Cambridge, MA 01239.

[1]In particular the Potts model exponents have been conjectured by M. P. M. den Nijs, J. Phys. A **12,** 1857 (1979); and supported by the renormalization group studies of B. Nienhuis, E. K. Riedel, and M. Schick, J. Phys. A **13,** L189, (1980); the Monte Carlo renormalization group studies of C. Rebbi and R. H. Swendsen, Phys. Rev. B **21,** 4094 (1980); and exact solution of a related model by R. J. Baxter, J. Phys. A **13,** L.61 (1980). The most relevant models (classes) for surface phenomena are the Ising (two-state Potts) model, the three-state Potts model, the four-state Potts model and the X-Y model with cubic anisotropy. The q-state Potts model consists of an array of spins which are coupled (attractively) by nearest-neighbor interactions and can point in q different directions. The X-Y model has continuous symmetry and continuously varying critical exponents.
[2]L. P. Kadanoff and Alan C. Brown, Ann. Phys. **121,** 318 (1979).
[3]S. Fain and M. Schick, J. Vac. Sci. Technol. **18,** 501 (1981), these proceedings, Pt. I
[4]See for example, R. Brout, *Phase Transitions* (Benjamin, New York, 1965); Kerson Huang, *Statistical Mechanics* (Wiley, New York, 1963).
[5]C. G. Shaw, S. C. Fain, Jr., and M. D. Chinn, Phys. Rev. Lett. **41,** 955 (1978). The antiphase domains seen in chemisorbed overlayers can be described as incommensurate structures with walls so thin that no adatom sits in a "bad" site. M. Shick, private communication.
[6]The transitions (and "ordered" states) in such an "unconstrained" lattice gas are very different from those we shall discuss. See for example D. R. Nelson and B. I. Halperin, Phys. Rev. B **19,** 2459 (1979).
[7]A. N. Berker, S. Ostlund, and F. A. Putnam, Phys. Rev. B **17,** 3650 (1978).
[8]T. L. Einstein and J. R. Schrieffer, Phys. Rev. B **7,** 3629 (1973).
[9]T. L. Einstein, CRC Crit. Rev. Solid State Mater. Sci. **7,** 261 (1978).
[10]E. D. Williams, S. L. Cunningham, and W. H. Weinberg, J. Chem. Phys. **68,** 4688 (1978).
[11]W.-Y. Ching, D. L. Huber, M. G. Lagally, and G.-C. Wang, Surf. Sci. **77,** 550 (1978).
[12]L. D. Roelofs, Robert L. Park, and T. L. Einstein, J. Vac Sci. Technol. **16,** 478 (1979).
[13]G. Doyen, G. Ertl, and M. Plancher, J. Chem. Phys. **62,** 2957 (1975).
[14]T. E. Felter, R. A. Barker, and P. J. Estrup, Phys. Rev. Lett. **38,** 1138 (1977); R. A. Barker and P. J. Estrup, Phys. Rev. Lett. **41,** 1307 (1978); P. J. Estrup, J. Vac. Sci. Technol. **16,** 635 (1979).
[15]D. A. King and G. Thomas, Surf. Sci. **92,** 201 (1980).
[16]G. Gewinner, J. C. Peruchetti, A. Jaegle, and R. Riedinger, Phys. Rev. Lett. **43,** 935 (1979).
[17]K. H. Lau and S. C. Ying, Phys. Rev. Lett. **44,** 1222 (1980).
[18]P. H. Holloway and J. B. Hudson, Surf. Sci. **43,** 123, 141 (1974).
[19]A. R. Kortan, P. I. Cohen, and Robert L. Park, J. Vac. Sci. Technol. **16,** 541 (1979).
[20]E. Bauer, in *Phase Transitions in Surface Films,* edited by J. G. Dash and J. Ruvalds, (Plenum, New York, 1980), p. 267.
[21]A. R. Kortan, Ph.D. Thesis, University of Maryland (1980).
[22]A discussion and references are given by J. G. Dash, *Films on Solid Surfaces* (Academic, New York, 1975), especially Chaps. 3 and 7.
[23]J. K. Kjems, L. Passell, H. Taub, J. G. Dash, and A. D. Novaco, Phys. Rev. B **13,** 1446 (1976).
[24]P. M. Horn, R. J. Birgeneau, P. Heiney, and E. M. Hammonds, Phys. Rev. Lett. **41,** 961 (1978).
[25]S. C. Fain, Jr., M. D. Chinn, and R. D. Diehl, Phys. Rev. B **21,** 4170 (1980); and C. G. Shaw and S. C. Fain, Jr., Surf. Sci. **83,** 1 (1979).
[26]A. E. Ferdinand and M. E. Fisher, Phys. Rev. **185,** 185 (1969); M. E. Fisher and M. N. Barber, Phys. Rev. Lett. **28,** 1516 (1972); D. P. Landau, Phys. Rev. B **13,** 2997 (1976).
[27]M. G. Webb and M. G. Lagally, Solid State Phys. **28,** 301 (1973); M. Fink and J. Ingram, Atomic Data **4,** 1 (1972).
[28]T. L. Einstein and L. D. Roelofs (unpublished).
[29]T.-M. Lu, G.-C. Wang, and M. G. Lagally, Phys. Rev. Lett. **39,** 411 (1977). G.-C. Wang, T.-M. Lu, and M. G. Lagally, J. Chem. Phys. **69,** 479 (1978).
[30]L. D. Roelofs, Ph.D. Thesis, University of Maryland (1980).
[31]P. M. Marcus, J. E. Demuth, and D. W. Jepsen, Surf. Sci. **53,** 501 (1975).
[32]John L. Cardy, M. Nauenberg, and D. J. Scalapino, preprint NSF-ITP-80-04.
[33]A preliminary version of this phase diagram is included in Robert L. Park,

T. L. Einstein, A. R. Kortan, and L. D. Roelofs in *Ordering in Two Dimensions*, edited by S. K. Sinha, (Elsevier North Holland, Amsterdam, 1980), 17. Fig. 5 includes an extension of the phase diagram to lower temperatures and coverages.

[34]E. Domany and M. Schick, Phys. Rev. B **20,** 3828 (1979); E. Domany, M. Schick, J. S. Walker, and R. B. Griffiths, Phys. Rev. B **18,** 2209 (1978); E. Domany, M. Schick, and J. S. Walker, Phys. Rev. Lett. **38,** 1148 (1977).

[35]M. E. Fisher and R. J. Burford, Phys. Rev. **156,** 583 (1967).

[36]Robert L. Park, J. E. Houston, and D. G. Schreiner, Rev. Sci. Instrum. **42,** 60 (1971).

[37]The correct choice involves varying the scattering wave vector $q = 2\mathbf{k}\sin\theta$ where $\mathbf{k}$ is the incident wave vector and θ the diffraction angle, while to measure the I–V profile E and θ are varied simultaneously in such a manner as to fix q.

[38]P. R. Bevington, *Data Reduction and Error Analysis for the Physical Sciences* (McGraw-Hill, New York, 1969).

[39]We always fit to a positive exponent form, inverting the data to be fit if necessary. For example, for the correlation length the exponent is expected to be $-\nu$ where $\nu > 0$. We accordingly fit the *inverse* correlation length using the exponent $+\nu$.

[40]This correspondence was realized for the analogous relation between the three-state Potts model and the $(\sqrt{3}\times\sqrt{3})R30°$ overlayer by S. Alexander, Phys. Lett. A **54,** 353 (1975).

[41]M. E. Fisher, Phys. Rev. **176,** 257 (1968). (FR refers to a singular rescaling of the temperature scale resulting from a constraint on a quantity which would ordinarily vary in a singular fashion through the transition. The result is that all the exponents are divided by the factor $(1-\alpha)$ where α is the specific heat exponent.)

[42]M. Nauenberg and D. J. Scalapino, Phys. Rev. Lett. **44,** 837 (1980).

[43]For $q > 4$, the Potts model exhibits a first-order phase transition. R. J. Baxter, J. Phys. C **6,** L445 (1973).

[44]P. Kleban (unpublished).